Geomechanics and Engineering, *Vol. 36, No. 2 (2024) 167-181*
https://doi.org/10.12989/gae.2024.36.2.167

Effect of relative stiffness on seismic response of subway station buried in layered soft soil foundation

Min-Zhe Xu, Zhen-Dong Cui* and Li Yuan

State Key Laboratory of Intelligent Construction and Healthy Operation & Maintenance of Deep Underground Engineering, School of Mechanics and Civil Engineering, China University of Mining and Technology, Xuzhou, Jiangsu, 221116, P.R. China

(*Received October 9, 2023, Revised November 25, 2023, Accepted January 2, 2024*)

Abstract. The soil-structure relative stiffness is a key factor affecting the seismic response of underground structures. It is of great significance to study the soil-structure relative stiffness for the soil-structure interaction and the seismic disaster reduction of subway stations. In this paper, the dynamic shear modulus ratio and damping ratio of an inhomogeneous soft soil site under different buried depths which were obtained by a one-dimensional equivalent linearization site response analysis were used as the input parameters in a 2D finite element model. A visco-elasto-plastic constitutive model based on the Mohr-Coulomb shear failure criterion combined with stiffness degradation was used to describe the plastic behavior of soil. The damage plasticity model was used to simulate the plastic behavior of concrete. The horizontal and vertical relative stiffness ratios of soil and structure were defined to study the influence of relative stiffness on the seismic response of subway stations in inhomogeneous soft soil. It is found that the compression damage to the middle columns of a subway station with a higher relative stiffness ratio is more serious while the tensile damage is slighter under the same earthquake motion. The relative stiffness has a significant influence on ground surface deformation, ground acceleration, and station structure deformation. However, the effect of the relative stiffness on the deformation of the bottom slab of the subway station is small. The research results can provide a reference for seismic fortification of subway stations in the soft soil area.

Keywords: layered soft soil foundation; seismic response; soil-structure interaction; soil-structure relative stiffness; subway station

1. Introduction

With the rapid urbanization and the increasingly serious traffic congestion in China, subway stations play a more and more important role in alleviating traffic pressure and improving people's lives. In recent years, the urban underground space has been developed rapidly and many subway stations have been built in China. The Yangtze River Delta is one of the most developed areas in China, with dense subway lines and many subway stations buried in the soft soil foundation. In the past, due to the constraints of the surrounding soil and rock, the seismic performance of subway stations was generally considered to be much better than that of ground structures (Lu and Hwang 2019). However, several recent severe earthquakes resulted in serious damage of underground structures, such as the Kobe earthquake (Iida *et al.* 1996), the 1999 Chi-Chi earthquake (Wang *et al.* 2001), and the 2008 Wenchuan earthquake (Yu *et al.* 2016). In particular, the Daikai station destroyed in the Kobe earthquake has attracted many researchers' attention to the seismic performance of underground structures. Due to the smaller constraint of soft soil, the underground structure in soft soil foundation may suffer more serious damage under the action of earthquake than that in the hard soil foundation and the rock strata (Gao *et al.* 2022). Therefore, it is necessary to study the deformation and failure mechanism of subway stations in soft soil foundation under the earthquake action.

The seismic response of underground structures in soft soil sites was studied by many researchers (Zhang and Cui 2017, Cheng and Sun 2018, Tang *et al.* 2020, Miao *et al.* 2020, Chou and Lin 2020, Wu *et al.* 2021, Li *et al.* 2021, Huynh *et al.* 2021, Ebadi-Jamkhaneh *et al.* 2021, Jiménez *et al.* 2022, Jaber *et al.* 2023). Cui *et al.* (2023) investigated the seismic response of a shallowly buried subway station in an inhomogeneous clay site based on numerical simulations and found the damage to subway stations was more serious in the inhomogeneous clay site than that in the homogeneous clay site under the same seismic wave. The soft soil subjected to ground motions showed the characteristics of filtering high-frequency waves and amplifying low-frequency waves (Chen *et al.* 2015). Besides, the soft soil layer generally strengthened the internal forces and deformations induced by earthquakes (Sun *et al.* 2020). Furthermore, the change of physical and mechanical behavior of soft soil greatly affects the seismic performance of underground structures (Cui *et al.* 2023). In general, the deformation of soft soil sites has a detrimental impact on the seismic performance of subway stations.

The soil-structure relative stiffness was widely regarded to be one of the key factors affecting the seismic response of underground structures (Wang and Munfakh 2001, Tsinidis 2017, Xu *et al.* 2019, Jiang *et al.* 2023). In previous

*Corresponding author, Professor
E-mail: cuizhendong@cumt.edu.cn

ISSN: 2005-307X (Print), 2092-6219 (Online)

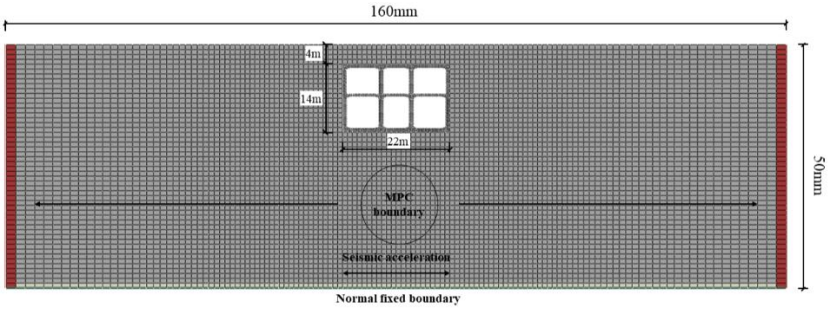

(a) Finite element model for the soil-structure interaction system

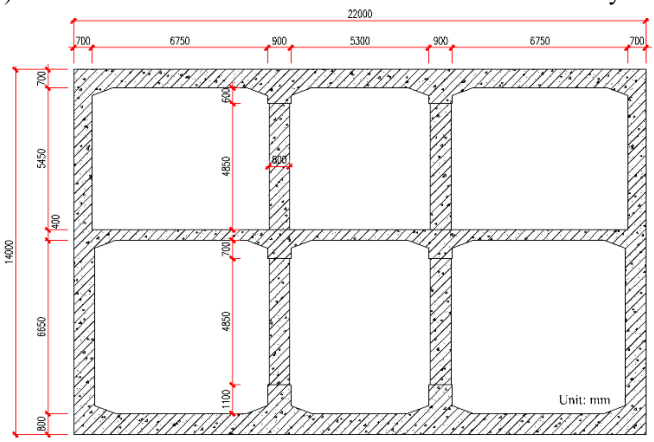

(b) Cross-sectional dimensions of the subway station

Fig. 1 Finite element model and cross-sectional dimensions of the subway station

studies, the concept of relative stiffness was paid attention by many researchers. Wang and Munfakh (2001) defined the relative stiffness of soil and structure by the ratio of the racking stiffness of the surrounding soil to that of the underground structure. Xu *et al.* (2019) found the horizontal relative deformation of the structure decreased monotonically with the increase of soil-structure flexibility ratio. Huo *et al.* (2006) found that the ratio of structural displacement to free field displacement was determined by the soil-structure relative stiffness and the form of the structure. Jiang *et al.* (2023) investigated the effect of parameters associated with soil-to-structure relative stiffness on seismic fragility curves of subway stations by a large number of subway stations with different cross-section sizes. The research results revealed the seismic performance of the structure with a higher relative stiffness ratio was relatively better, while there were special cases where some structures with a high relative stiffness ratio were more susceptible to failure under earthquake than structures with a lower relative stiffness ratio. Many scholars have conducted a series of research on the influence of relative stiffness on the seismic performance of underground structures, and have achieved rich research results. However, the definition of the relative stiffness ratio in previous studies only considers the relative stiffness of soil and structure in the horizontal direction. For underground structures, vertical earth pressure is one of the important parameters in the design of underground structures. The vertical earth pressure on the underground structure undergoes constant fluctuations during earthquakes (Wu *et al.* 2022). Moreover, the underground structure may float up under earthquake motions (Zhuang *et al.* 2015). Therefore, vertical relative stiffness should be considered in the study of relative stiffness. Furthermore, the current research on relative stiffness rarely takes into account the inhomogeneity of soil, and the method of reflecting relative stiffness by changing the elastic modulus of the concrete in the structure has some limitations due to the constant elastic modulus of concrete.

In this paper, the horizontal and vertical stiffness ratios were defined respectively to study the effects of horizontal and vertical relative stiffness on the seismic response of subway station. A two-dimensional finite element model for soil-structure dynamic interaction was established, and the relationship between the equivalent elastic modulus of the middle columns and the longitudinal spacing of columns in the two-dimensional model was derived. Based on the numerical simulation results, the deformation and damage of the subway station are discussed respectively, considering different soil-structure relative stiffness.

2. Numerical models

2.1 Soil and station models

A two-dimensional finite element model was established by ABAQUS, consisting of a two-story and three-span subway station and the surrounding inhomogeneous soft soil site, as shown in Fig. 1. To eliminate the influence of truncated boundaries on the seismic response of the subway station, the width of the site soil should be taken more than 7

Table 1 Properties of soils surrounding the subway station

Soil profiles	Thickness (m)	G_{dmax} (MPa)	Density ρ (kg/m^3)	Cohesion c (kPa)	Friction angle φ (°)	Poisson's ratio υ
Clay	30	1.56~65.60	1840	7.1	27.5	0.499
Sand	20	217.80	2000	0.0	34.5	0.3

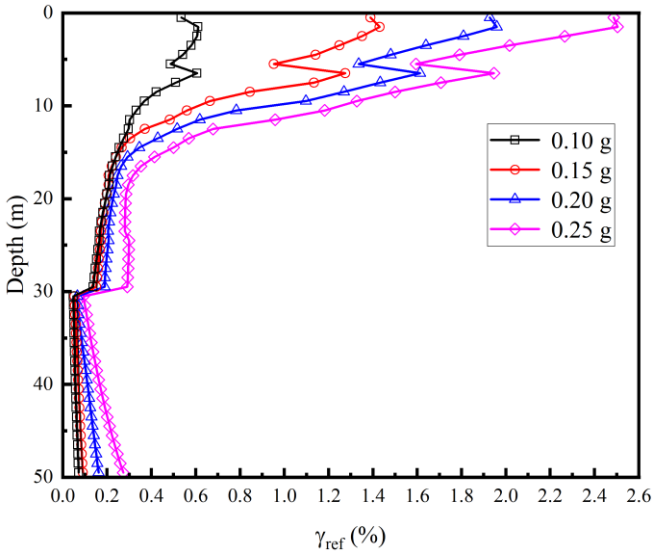

Fig. 2 Variations of the reference shear strain with depth under different PGAs

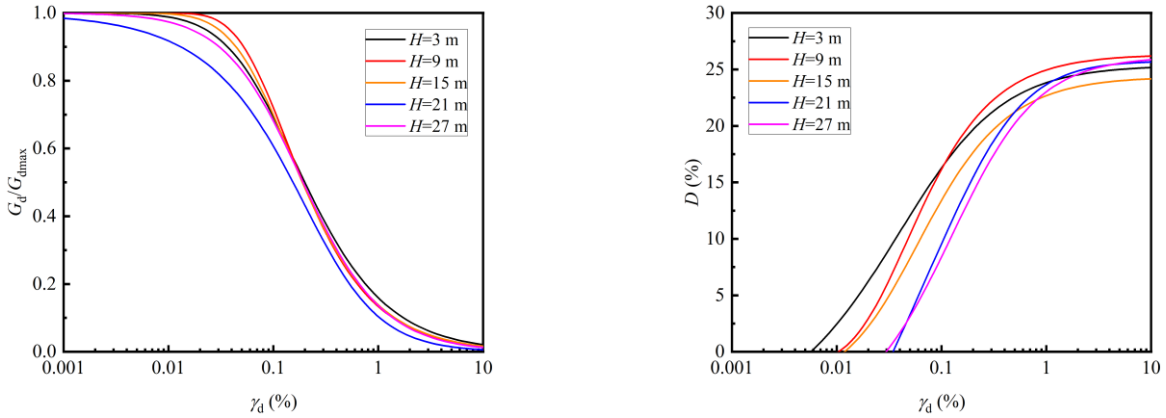

(a) G_d/G_{dmax} ~ γ_d (b) D ~ γ_d

Fig. 3 Variations of dynamic shear modulus ratio and damping ratio with shear strain for clay under different buried depths

times the width of the subway station (Xu *et al*. 2019). The soft soil site is 160 m in width and 50 m in height, and the subway station is buried at 4 m in depth, as shown in Fig. 1(a). The subway station is 14 m in height and 22 m in width and the cross-section of the middle columns is rectangular, with a length of 4.85 m and a width of 0.8 m, as shown in Fig. 1(b). To consider the inhomogeneity caused by the stratification and consolidation of soil under natural conditions, the model site is composed of 30 m clay and 20 m sand, in which the maximum dynamic shear modulus of clay varies with the buried depth according to the formula fitted by Cui et al. (2023), as shown in Eq. (1). The water table is assumed to at the ground surface. The physical and mechanical parameters of soil layers are summarized in Table 1.

$$\lg G_{dmax} = 0.46803 + 0.91772 \times \lg H \tag{1}$$

where G_{dmax} is the maximum dynamic shear modulus of clay; H is the burial depth of soil.

In this numerical model, the 4-node bilinear full-integration plane strain elements are used to mesh the model site and the subway station structure. The rebars are meshed by 2D beam elements and embedded into the concrete. The bottom boundary of the model is fixed in the normal direction. The multi-point constraint (MPC) is assigned in the lateral boundaries to simulate the horizontal vibration effect during seismic propagation (Bao *et al.* 2017, Chen *et al.* 2023, Chen *et al.* 2023). The damage plasticity model is used to simulate the

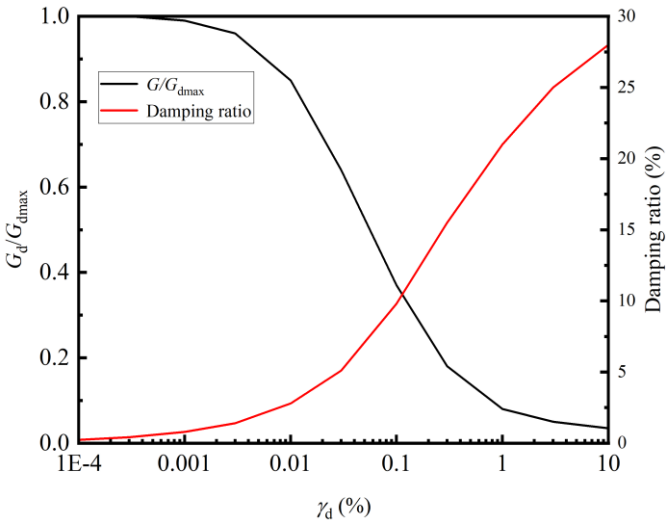

Fig. 4 Variations of dynamic shear modulus ratio and damping ratio with shear strain for sand

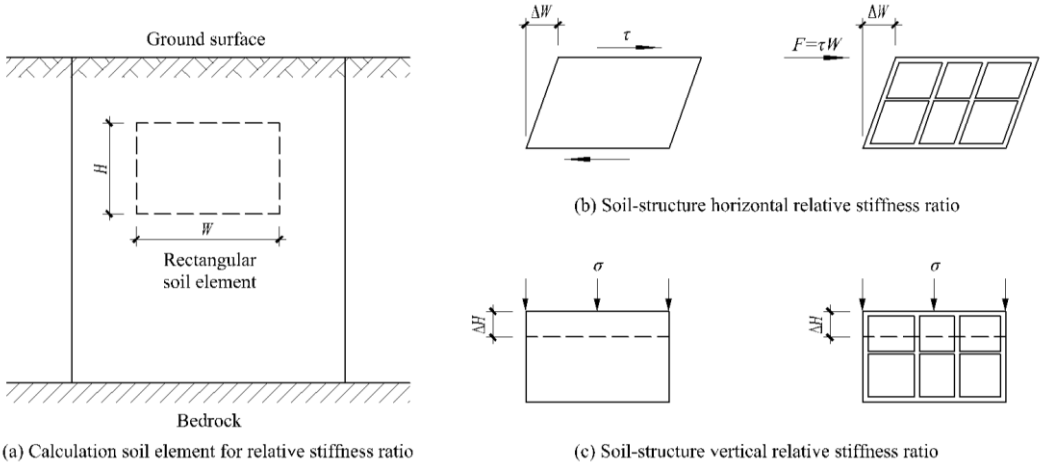

Fig. 5 Soil-structure relative stiffness ratios

nonlinear behavior of concrete. For the contact relationship between soil and structure, the normal direction of the contact surface is set as hard contact. When there is tension between soil and structure, the contact surface will separate immediately. The tangential direction of the contact surface follows the Coulomb friction criterion. The critical shear stress of the contact surface can be expressed as

$$\tau_{\text{critical}} = \mu\sigma \tag{2}$$

where μ is the friction coefficient of the contact surface, taken as 0.4 in this paper (Huo *et al.* 2005, Bobet *et al.* 2008, Gomes 2013, Ma *et al.* 2019); σ is the normal contact stress on the contact surface.

To consider the nonlinear behavior of soil, the dynamic elastic modulus ratio and damping ratio corresponding to the reference shear strain at different depths can be obtained by the frequency-domain equivalent linear method. The equivalent linear seismic response of a one-dimensional site was analyzed by DEEPSOIL to obtain the reference shear strain of soil at different depths. The reference shear strain along the depth under different peak ground motions is shown in Fig. 2. According to Cui *et al.* (2023), the variations of dynamic shear modulus ratio and damping ratio with the shear strain for clay under different buried depths are shown in Fig. 3. The variations of dynamic shear modulus ratio and damping ratio of sand with shear strain are shown in Fig. 4 (Seed and Idriss 1970).

2.2 Relative stiffness ratios

Due to the inability of the two-dimensional model to reflect the spatial distribution of the columns, the two rows of middle columns must be considered equivalent to the two walls along the longitudinal direction of the station. According to the principle of equivalent stiffness, the equivalent walls are required to have the same lateral deformation stiffness as the middle columns (Zhuang *et al.* 2015). Therefore, the equivalent elastic modulus of concrete E_{eq} for the middle columns can be calculated by

$$E_{\text{eq}} = \frac{E_c b}{L} \tag{3}$$

where E_c is the elastic modulus of concrete; b is the

Table 2 Different soil-structure relative stiffness cases

Longitudinal column distance (m)	Equivalent elastic modulus of middle column (GPa)	K_h (kN/mm)	R_h	K_v (kN/mm)	R_v
6	5.00	25.39	1.63	1395.81	0.09
8	3.75	22.90	1.81	1194.71	0.10
10	3.00	21.07	1.97	1045.49	0.12
12	2.50	19.66	2.11	930.65	0.13

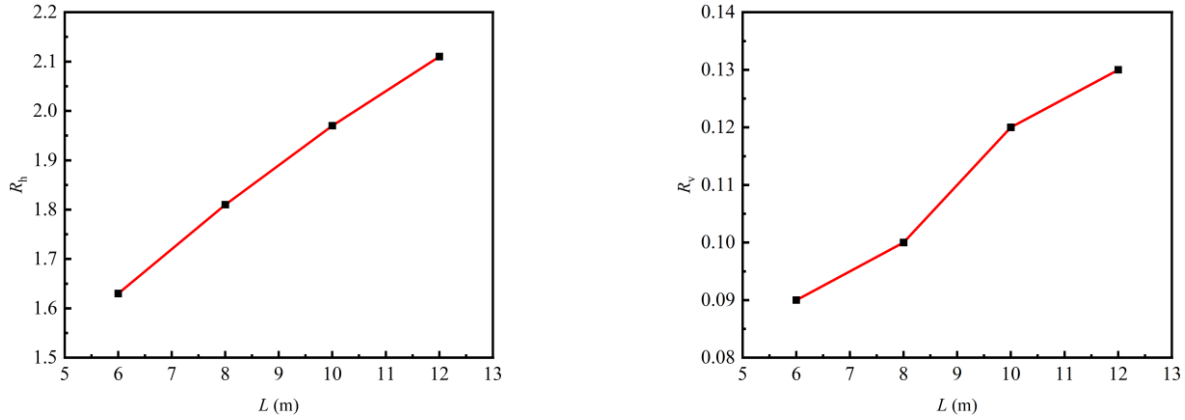

(a) Horizontal relative stiffness ratio (b) Vertical relative stiffness ratio

Fig. 6 Variations of horizontal relative stiffness ratio and vertical relative stiffness ratio with longitudinal spacing of middle columns

longitudinal width of the column section, taken as 1 m in this paper; L is the longitudinal column spacing.

In order to reflect the relative stiffness of soil and structure, the relative stiffness ratios are defined as shown in Fig. 5. The horizontal stiffness ratio R_h (Wang and Munfakh 2001) and vertical stiffness ratio R_v are determined by Eqs. (4) and (5), respectively.

$$R_h = \frac{G_s W}{H K_h} \tag{4}$$

$$R_v = \frac{E_s W}{H K_v} \tag{5}$$

where G_s is the shear modulus of soil; E_s is the elastic modulus of soil; W is the width of the subway station; H is the height of the subway station; K_h is the horizontal stiffness of the structure; K_v is the vertical stiffness of the structure.

To meet the actual engineering situation, four types of station structures with longitudinal column distances of 6 m, 8 m, 10 m and 12 m were selected. The equivalent elastic modulus of the middle columns of the four station structures was calculated by Eq. (3). The horizontal and vertical stiffness of four kinds of station structures were determined by the numerical calculation. Different soil-structure relative stiffness models are summarized in Table 2. Fig. 6 illustrates the variations of horizontal relative stiffness ratio and vertical relative stiffness ratio with the longitudinal spacing of middle columns. There is a positive correlation between the soil-structure relative stiffness ratio and the longitudinal column distance.

2.3 Modal analysis

Modal analysis of soil and structure models was usually required before dynamic time history analysis. The damping coefficient of the station structure was calculated with the modal damping ratio of 3% (Zhuang *et al.* 2015). The equivalent viscous damping ratio of soil at different depths was used to calculate the damping coefficient of soil. Rayleigh damping was a common and effective damping in numerical analysis, which was regarded to be a linear combination of mass and stiffness matrices of the system with two constants, expressed as

$$C = \alpha M + \beta K \tag{6}$$

where C, M and K are the damping, mass and stiffness matrices of soil, respectively; α and β are the Rayleigh damping coefficients. The Rayleigh damping coefficients can be written as

$$\begin{aligned} \alpha &= \frac{2\xi_i \omega_m \omega_n}{\omega_m + \omega_n} \\ \beta &= \frac{2\xi_i}{\omega_m + \omega_n} \end{aligned} \tag{7}$$

where ω_m and ω_n are the first and second target frequencies, respectively; ξ_i is the equivalent viscous damping ratio.

2.4 Input ground motion

The selection and input of the seismic wave were critical

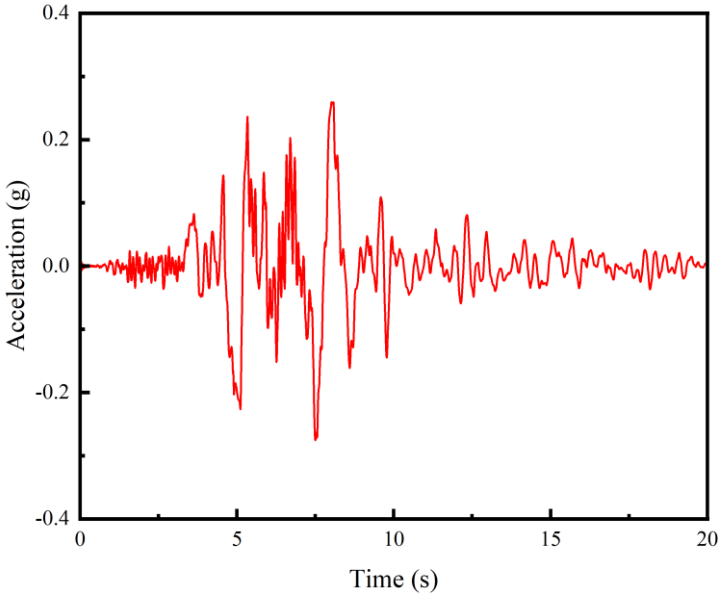

Fig. 7 Kobe motion

steps in seismic response analysis. Due to the influence of noise and other factors, seismic waves were processed for the seismic analysis. The seismic waves recorded by Kobe University were used in this study. The first 20 s of the prototype seismic recording which was processed by baseline correction was selected as the input ground motion by filtering and scaling to match the peak ground accelerations (PGAs) of 0.1 g, 0.15 g, 0.2 g and 0.25 g, respectively. The earthquake record from Kobe University is shown in Fig. 7.

3. Numerical results and discussions

3.1 Displacement of ground surface

Fig. 8 illustrates the variations of ground vertical displacement with ground horizontal positions for different vertical stiffness ratios under the input PGAs of 0.1 g, 0.15 g, 0.2 g and 0.25 g, respectively. Under the PGA of 0.1 g, the curves of ground vertical displacements are in the type of "W", as shown in Fig. 8(a). There are some extreme points in these displacement curves, with four minimum points and three maximum points. The minimum points are located at 67 m, 73 m, 87 m and 93 m and the maximum points are located at 70 m and 90 m, respectively. With the increase of the vertical stiffness ratio, the vertical displacement above the center of the station is 5.71 mm, 3.40 mm, 1.01 mm and -1.64 mm, respectively. The upward displacement of the ground surface decreases gradually with the vertical stiffness ratio increasing. When the vertical stiffness ratio is 0.13, the subsidence of the ground surface occurs. Under the PGA of 0.15 g, with the increase of vertical stiffness ratio, the vertical displacements above the station center are 8.34 mm, 3.58 mm, -1.56 mm and -7.37 mm, respectively, as shown in Fig. 8(b). When the vertical stiffness ratios are 0.09 and 0.10, the ground surface upward displacements are 46.06% and 5.29% larger than that under PGA = 0.1 g, respectively. The surface subsidence occurs when the vertical stiffness ratio is 0.12. The ground surface settlement is 4.49 times larger than that under PGA = 0.1 g when the vertical stiffness ratio is 0.13. Under the PGA of 0.2 g, the vertical displacements above the station center are 11.41 mm, 3.11 mm, -6.92 mm and -44.79 mm, respectively as the vertical stiffness ratio increases, as shown in Fig. 8(c). When the vertical stiffness ratio is 0.09, the ground surface displacement continues to increase compared with that under the PGAs of 0.1 g and 0.15 g. However, the upward displacement of the ground surface begins to decrease with R_v = 0.10. When the vertical stiffness ratios are 0.12 and 0.13, the ground surface settlements increase compared with that under the PGAs of 0.1 g and 0.15 g. The curve of the settlement with R_v = 0.13 is in the type of "U". Under the PGA of 0.25 g, with the increase of vertical stiffness ratio, the vertical displacements above the station center are 13.83 mm, 0.91 mm, -31.6 mm and -82.47 mm, respectively, as shown in Fig. 8(d). The changing trend of displacements is consistent with that under PGA = 0.2 g.

The variations of ground vertical displacement above the center of the station with the PGA for different vertical relative stiffness ratios are shown in Fig. 9. The vertical displacement increases linearly with PGA when R_v is 0.09. For R_v = 0.10, the variation amplitude of vertical displacement is relatively small with the PGA increasing from 0.1 g to 0.25 g. When the vertical stiffness ratios are 0.12 and 0.13, the ground surface settlement develops rapidly when the PGA increases from 0.1 g to 0.25 g. The variation of land surface settlement with R_v = 0.13 is larger than that with R_v = 0.12. It can be concluded from the results that the ground surface with higher vertical stiffness ratio is more likely to settle than that with lower vertical stiffness ratio. The ground subsidence may be caused by the loss of the bearing capacity of the subway station columns due to the increase of the peak acceleration of ground motion.

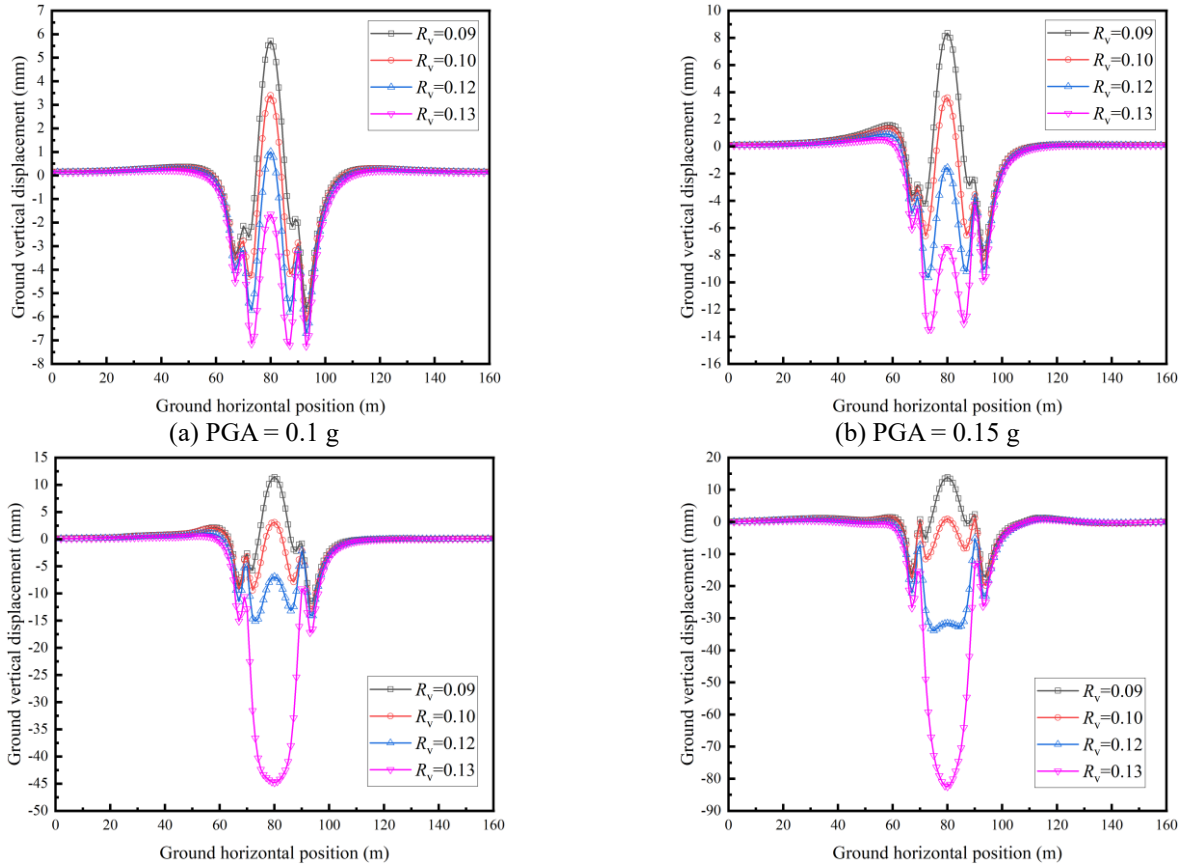

(a) PGA = 0.1 g (b) PGA = 0.15 g

(c) PGA = 0.2 g (d) PGA = 0.25 g

Fig. 8 Variations of ground vertical displacement with ground horizontal positions for different vertical relative stiffness ratios under different PGAs

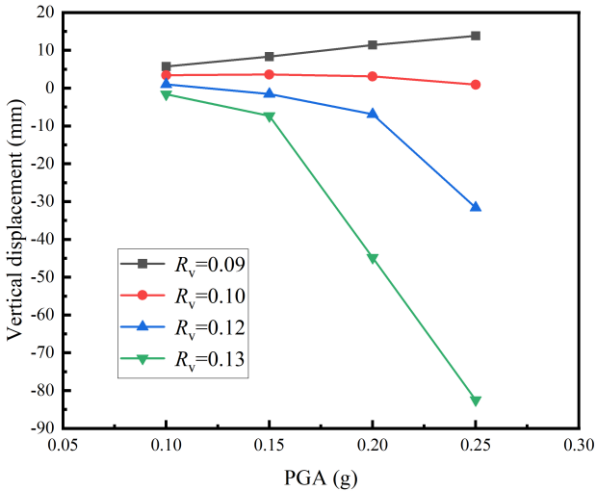

Fig. 9 Variations of ground vertical displacement above the center of the station with the PGA for different vertical relative stiffness ratios

3.2 Near-field acceleration response

In order to study the effect of the soil-structure relative stiffness on the near-field acceleration, observation points 1, 2 and 3 are assigned around the station, as presented in Fig. 10. The variations of the maximum horizontal acceleration of the observation points along the height under different PGAs are shown in Fig. 11. When PGA = 0.1 g, there is no obvious difference for the variation of acceleration with height among different horizontal stiffness ratios, and the acceleration increment of the soil around the upper floor of the structure is larger than that of the lower floor, as shown in Fig. 11(a). When the PGA is larger than 0.1 g, the acceleration decreases first and then increases along the

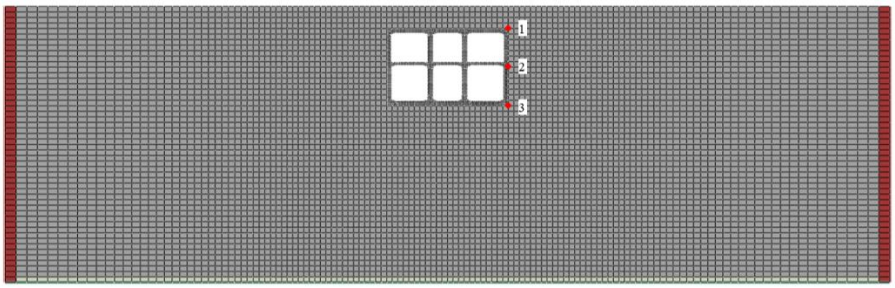

Fig. 10 Location of site acceleration observation points

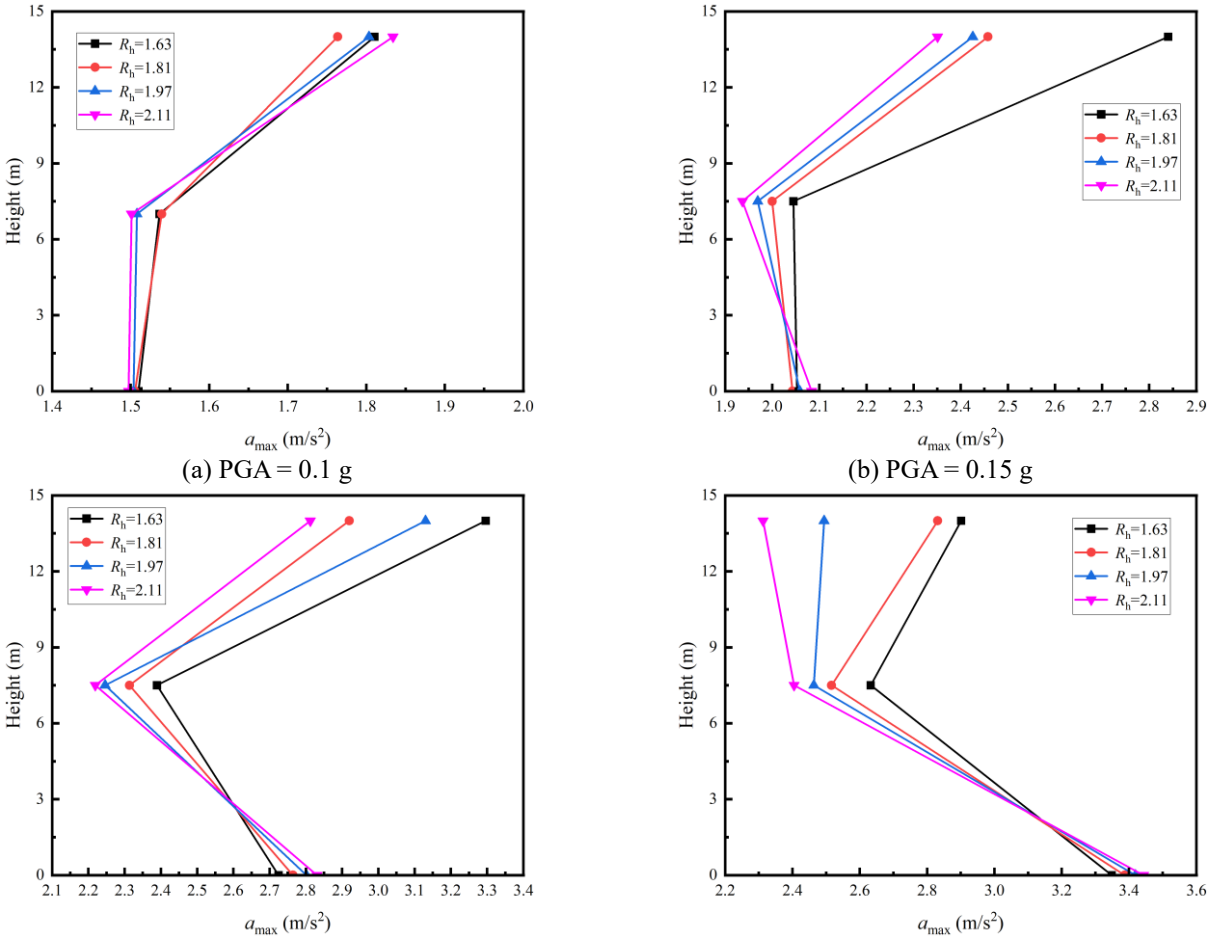

(a) PGA = 0.1 g (b) PGA = 0.15 g

(c) PGA = 0.2 g (d) PGA = 0.25 g

Fig. 11 Variations of maximum acceleration of the observation points with height for different horizontal relative stiffness ratios under different PGAs

height, as shown in Figs. 11(b)-11(d). The difference among the variations of acceleration along height under different horizontal stiffness ratios is more obvious with the increase of PGA. In this study, the acceleration magnification is defined as the ratio of the maximum acceleration value at observation point 1 to the maximum acceleration value at observation point 3. Fig. 12 shows the variations of acceleration magnification with horizontal relative stiffness ratio under different PGAs. When PGA is less than or equal to 0.15 g, the acceleration magnification is larger than 1, which means that the acceleration is amplified. When PGA = 0.2 g, the acceleration magnification with the R_h less than 2.11 is larger than 1, while that with R_h = 2.11 is less than 1. When PGA = 0.25 g, the acceleration magnifications under four horizontal relative stiffness ratios are less than 1. Besides, the horizontal relative stiffness has different effects on acceleration amplification under different PGAs. The acceleration magnification showed a slowly increasing trend when PGA = 0.1 g. However, when PGA is larger than 0.1 g, the acceleration magnification decreases rapidly with the increase of horizontal stiffness ratio.

From the above analysis, it can be concluded that under strong earthquakes, the acceleration magnification of the site around the subway station decreases with the increase

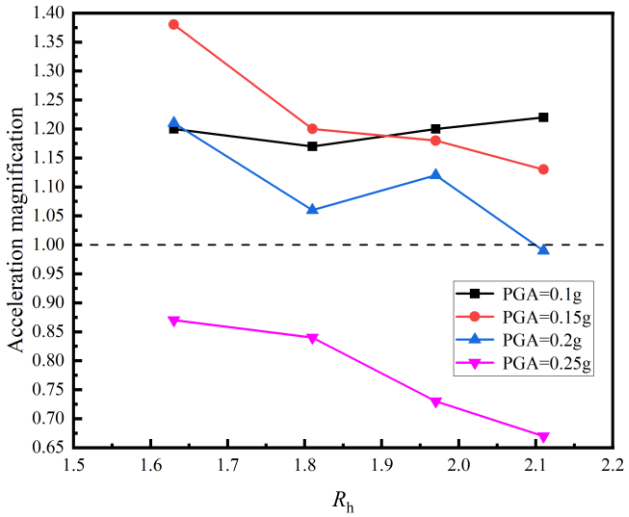

Fig. 12 Variations of acceleration magnification with horizontal relative stiffness ratio under different PGAs

of the horizontal stiffness ratio. The increase in ground motion causes the acceleration magnification to be less than 1. The reason for this phenomenon may be due to the reduction of station structure stiffness. When PGA = 0.1 g, the effect of horizontal relative stiffness on near-field acceleration can be ignored in the seismic design of underground structures. However, when PGA is higher than 0.1 g, the relative stiffness has a significant effect on the acceleration.

3.3 Damage of subway station

The failure of the structures with different longitudinal column spacing was analyzed based on tensile and compressive damage factors to study the influence of relative stiffness on the damage of the subway station under earthquake. Fig. 13 illustrates the tensile and compression damage distributed contour diagrams of the subway station with different relative stiffness under PGA = 0.1 g. The compression damage of the structure is mainly observed at the end of the middle columns and the end of the middle slabs, especially the former one. Slight compression damage is observed at the joints between the sidewalls and the slabs. With the increase of the longitudinal column spacing of the station, the compression failure areas of the middle columns of the structure gradually extend from the ends of the columns to the middle, increasing the damage areas. This explains that the settlement in section 3.1 first appears on the ground surface with a large relative stiffness ratio. The tensile damage of the station structure mainly concentrates on the ends of the columns, the joints between the sidewalls and the slabs, and the ends of the middle slabs. The whole station suffers serious tensile damage, especially at the column ends. With the increase of the longitudinal distance between columns, the tensile damage areas at the ends of the column decrease, while the tensile damage areas at the joints between the sidewalls and the slabs increase.

In summary, under the same seismic wave, the ends of the middle column with a higher relative stiffness ratio will suffer more serious compression damage, while suffering less tensile damage. Moreover, the tensile damage at the joints between the sidewalls and the bottom slab increases with the relative stiffness increasing.

3.4 Horizontal relative displacement of sidewall

Under the action of the earthquake, the station sidewalls are subjected to horizontal seismic force and thus produce horizontal displacement. Fig. 14 shows the horizontal relative displacements of the station sidewalls after the earthquake with PGA = 0.1 g. After the earthquake, the maximum horizontal relative displacement of the left wall of the station occurs in the middle of the upper floor shown in Fig. 14(a), while the maximum horizontal relative displacement of the right wall of the station occurs in the middle of the lower floor shown in Fig. 14(b). With the increase of the horizontal stiffness ratio, the horizontal relative deformations of the left wall are 12.26 mm, 14.49 mm, 15.62 mm and 16.89 mm, respectively and those of the right wall are 8.41 mm, 10.12 mm, 11.49 mm and 13.13 mm, respectively. The horizontal relative deformation of station sidewalls increases with the R_h increasing. The relative deformation of the left wall with R_h = 2.11 is 37.77% larger than that of the left wall with R_h = 1.63, while the relative deformation of the right wall with R_h = 2.11 is 56.12% larger than that of the right wall with R_h = 1.63.

Fig. 15 illustrates the variations of the maximum horizontal relative displacements of the station sidewalls with the horizontal stiffness ratio under PGA = 0.1 g. The maximum horizontal relative displacements increase approximately linearly with the horizontal stiffness ratio increasing. As shown in Fig. 15, the change slopes of the left wall and the right wall are approximately 17.58 and 15.14, respectively, and the difference between the change slopes of the left and right walls is small because the left and right sidewalls of the station maintain synchronous deformation during the earthquake and the station structure maintains a parallelogram shape. In general, the relative stiffness has a significant influence on the deformation of station sidewalls, which should be considered in the seismic design.

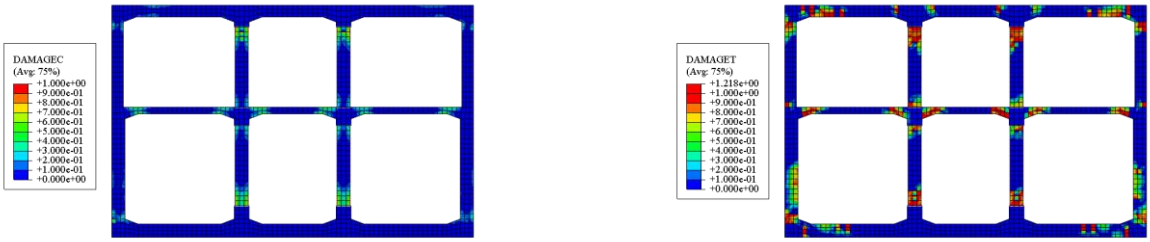

(a) Longitudinal column spacing 6 m

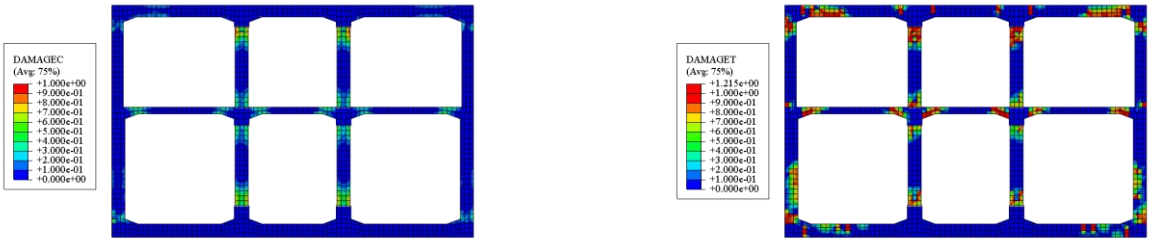

(b) Longitudinal column spacing 8 m

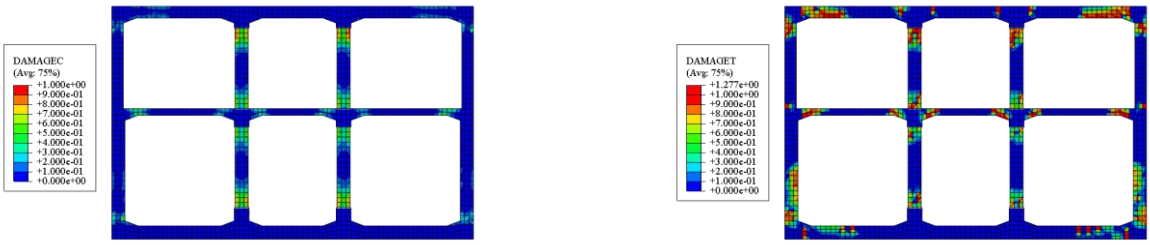

(c) Longitudinal column spacing 10 m

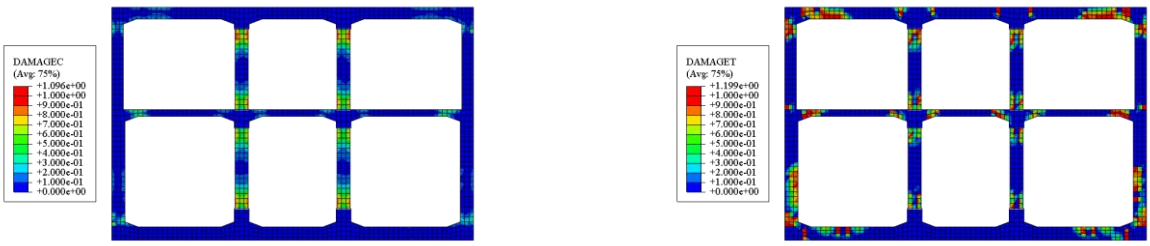

(d) Longitudinal column spacing 12 m

Fig. 13 Damage distributed contour diagrams of the subway station with different longitudinal middle column spacing

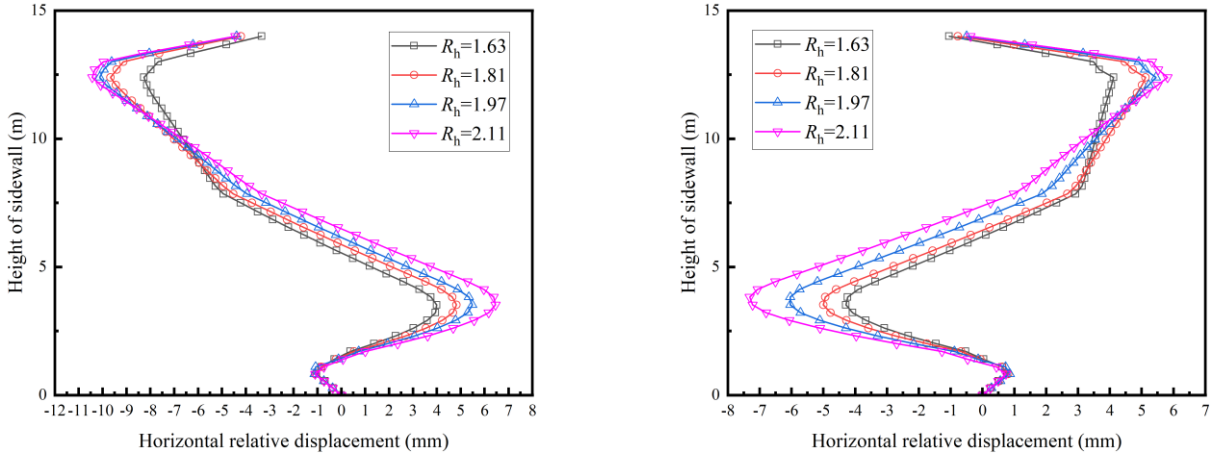

(a) Left sidewall (b) Right sidewall

Fig. 14 Horizontal relative displacements of the sidewalls after the action of 0.1 g seismic wave under different horizontal relative stiffness ratios

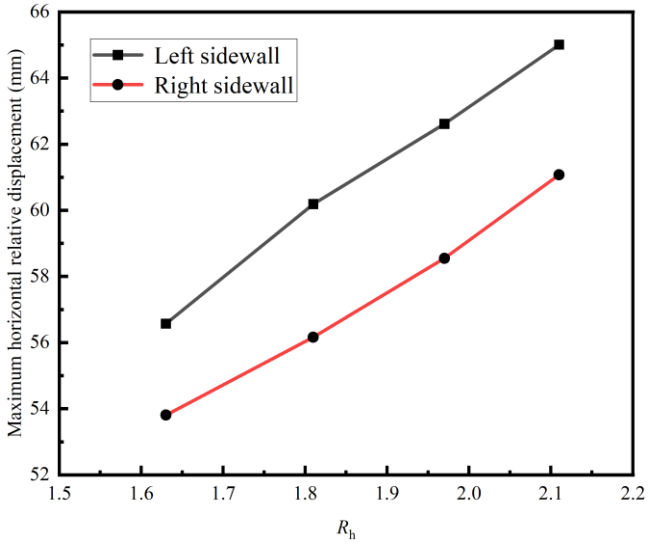

Fig. 15 Maximum horizontal relative displacements of the sidewalls with different horizontal relative stiffness ratios

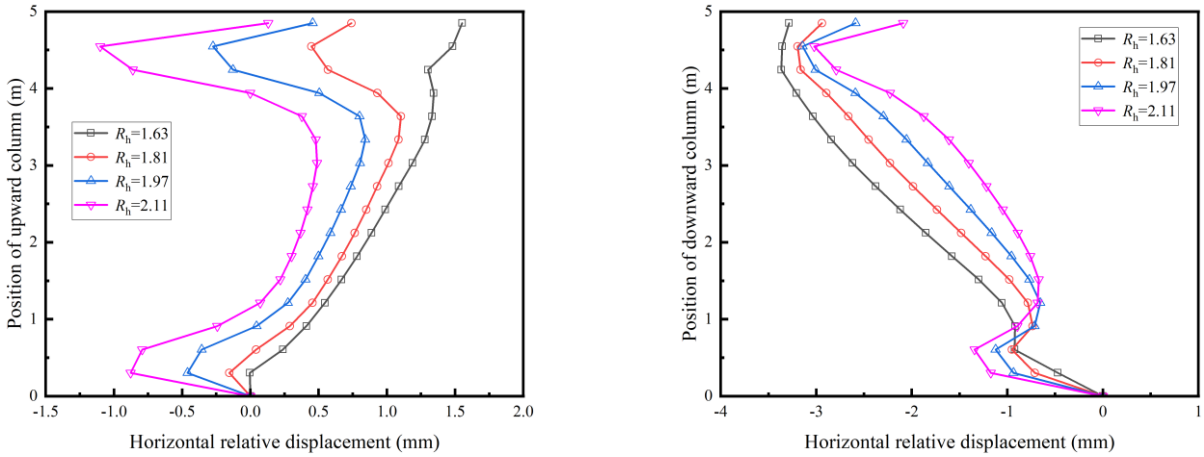

(a) Left column on the upper floor (b) Left column on the lower floor

Fig. 16 Horizontal relative displacements of the left middle columns after the action of 0.1 g seismic wave under different horizontal relative stiffness ratios

3.5 Deformation of middle column

The middle column is the key component of seismic resistance in subway stations. In order to investigate the horizontal deformation of the middle columns, the left middle columns of the subway station were selected for analysis. The horizontal relative displacements of the upper and lower left middle columns along the height are shown in Fig. 16. The left middle column of the upper floor of the station is inclined to the right and there exist abrupt changes at the ends of the middle column, as shown in Fig. 16(a).

The abrupt change amplitude of displacement increases with the horizontal stiffness ratio increasing, resulting from arching outward of the column surface due to the compression failure. With the increase of the horizontal stiffness ratio, the amplitude of the column tilting to the right decreases, resulting in less tensile failure, as concluded in Section 3.4. The middle column on the left side of the lower floor of the station is inclined to the left and the variations of the horizontal relative displacement with the height are the same as that of the left middle column of the upper floor, as shown in Fig. 16(b).

It is concluded that the increase of the horizontal stiffness ratio leads to greater compression failure at the end of the column and less tilt amplitude of the column under the same seismic wave. Therefore, the relative stiffness has a significant effect on the deformation of the column.

3.6 Horizontal relative displacement between slabs

Fig. 17 shows the time-history curves of horizontal relative displacements between the ceiling and the bottom slab with different horizontal stiffness ratios under PGA = 0.1 g. The maximum horizontal relative displacements with the R_h of 1.63, 1.81, 1.97 and 2.11 are 52.83 mm, 55.57 mm, 57.90 mm and 60.29 mm, respectively. The horizontal relative displacement increases 14.12% with the soil-structure horizonal relative stiffness ratio increasing from 1.63 to 2.11. Similar conclusions were drawn in a recent study (Xu *et al.* 2019). The maximum inter-story drift

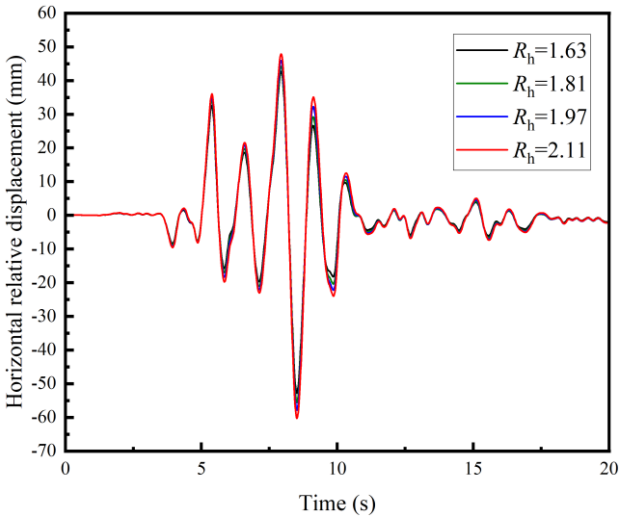

Fig. 17 Horizontal relative displacements between the ceiling and bottom slab with PGA = 0.1 g under different horizontal relative stiffness ratios

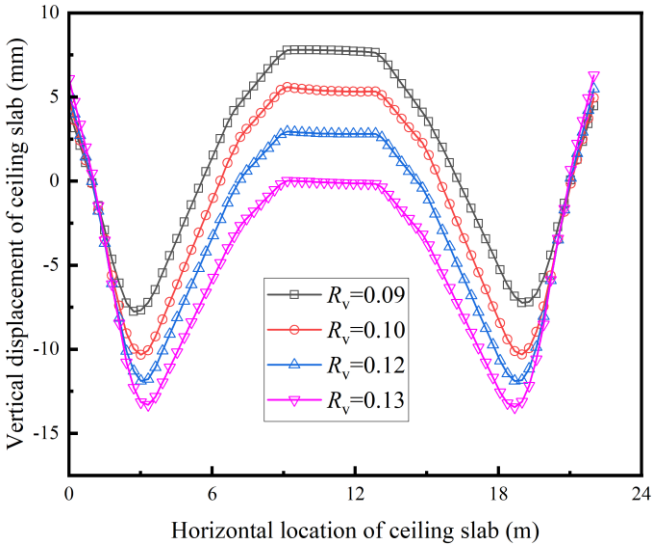

Fig. 18 Vertical displacements of the ceiling with PGA = 0.1 g under different vertical relative stiffness ratios

Table 3 Seismic performance levels of subway station

Seismic performance level	Structural behavior	Ultimate IDA
Level 1	Undamaged	$\theta_{max} \leq 1.2/1000$
Level 2	Slightly damaged	$1.2/1000 < \theta_{max} \leq 2.5/1000$
Level 3	Moderately damaged	$2.5/1000 < \theta_{max} \leq 4.0/1000$
Level 4	Severely damaged	$4.0/1000 < \theta_{max} \leq 6.0/1000$
Level 5	Destroyed	$\theta_{max} > 6.0/1000$

angles between the ceiling and the bottom slab are 3.77/1000, 3.97/1000, 4.14/1000 and 4.31/1000, respectively. The maximum inter-story drift angle with R_h = 2.11 is 14.32% larger than that with R_h = 1.63. According to Zhuang *et al.* (2019), the seismic performance levels of subway station is summarized in Table 3, in which the inter-story drift angle (IDA) is used as a quantitative criterion. The subway station is moderately damaged with the R_h of 1.63 and 1.81. When the R_h increase to 1.97, the station structure will be severely damaged. It can be illustrated from the results that the damage degree of subway station is related to the horizontal relative stiffness between soil and station structure.

3.7 Vertical displacement of structure

Fig. 18 illustrates the variations of the vertical displacements of the ceiling slab with its horizontal

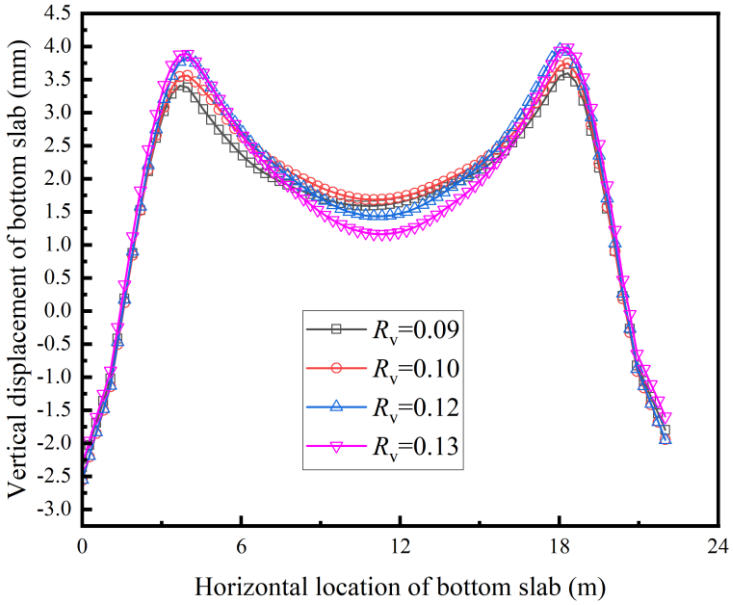

Fig. 19 Vertical displacements of the bottom slab with PGA = 0.1 g under different vertical relative stiffness ratios

locations for different vertical stiffness ratios under the PGA of 0.1 g. The curves of the vertical displacements of the ceiling are in the type of "W", which are approximately the same as those of the ground surface shown in Fig. 8, indicating that the ground surface settlement is mainly affected by the deformation of the ceiling of the station. The curves arch upward in the mid-span ceiling and depress downward in the left and right spans. The vertical displacements of the mid-span ceiling are 7.77 mm, 5.36 mm, 2.82 mm and -0.09 mm respectively as the R_v increases under the earthquake of PGA = 0.1 g. The maximum deformations of the side spans of the ceiling are -7.76 mm, -10.34 mm, -11.89 mm and -13.44 mm, respectively. The higher the vertical stiffness ratio, the smaller the vertical displacement of the ceiling. However, the maximum displacements of the ends of the ceiling increase with the vertical stiffness ratio increasing, which are 4.47 mm, 4.96 mm, 5.48 mm and 6.29 mm, respectively, resulting in the increase of the relative deformations of the ceiling, which are 12.23 mm, 15.30 mm, 17.37 mm and 19.73 mm, respectively. The relative deformation of the ceiling with R_v = 0.13 is 61.32% larger than that of the ceiling with R_v = 0.09. The results indicate that the increase of the vertical stiffness ratio results in the higher relative deformation of the ceiling.

Fig. 19 illustrates the variations of the vertical displacements of the bottom slab with its horizontal locations for different vertical stiffness ratios under the PGA of 0.1 g. The vertical displacement curves of the bottom slab show the shape of "M". The maximum vertical displacements occur in the right span of the bottom slab, which are 3.60 mm, 3.75 mm, 3.95 mm and 3.98 mm, respectively with the vertical stiffness ratio increasing. Moreover, the relative deformations of the bottom slab are 5.97 mm, 6.31 mm, 6.51 mm and 6.30 mm, respectively. Therefore, the relative stiffness has little influence on the relative deformation of the bottom slab.

4. Conclusions

In this paper, the soil-structure relative stiffness ratios were defined from the horizontal and vertical directions, respectively. The effect of relative stiffness on the seismic response characteristics of two-story three-span subway stations in inhomogeneous soft soil was investigated by the numerical simulation. In addition, the influence of the inhomogeneity of soil and the intensity of input ground motion were considered and quantitatively analyzed. The numerical results demonstrate that the soil-structure relative stiffness has a significant influence on the deformation of the structure and surrounding field. The main conclusions drawn from this study are as follows.

(1) The ground surface with higher soil-structure vertical stiffness ratio is more likely to settle than that with lower vertical stiffness ratio. When the PGA is less than or equal to 0.15 g, the curves of the ground vertical displacements exhibit a "W" shape. However, for the PGA greater than or equal to 0.2 g, the ground surface with the vertical stiffness ratio of 0.13 is in the type of "U".

(2) Under strong earthquakes, the acceleration magnification of the site surrounding the subway station decreases as the horizontal stiffness ratio increases. The difference among the accelerations under different horizontal stiffness ratios is more obvious with the PGA increasing. The influence of horizontal relative stiffness on near-field acceleration under strong earthquakes is greater than that under small earthquakes.

(3) When subjected to the same seismic wave, middle columns with higher relative stiffness ratios endure more severe compression damage but less tensile damage. Additionally, the relative stiffness affects the extent of tensile damage at the joints between the sidewalls and the bottom slab.

(4) The horizontal relative deformation of station sidewalls increases with the horizontal stiffness ratio

increasing, with the left wall experiencing a 37.77% greater deformation at R_h = 2.11 compared to R_h = 1.63, and the right wall showing a 56.12% larger deformation at R_h = 2.11 compared to R_h = 1.63. In addition, the maximum horizontal relative displacements of the sidewalls increase approximately linearly as the horizontal stiffness ratio increases.

(5) After the earthquake, the left middle column of the lower floor is inclined to the right, while the middle column on the left side of the upper floor is inclined to the left. The increase of the horizontal stiffness ratio leads to greater compression failure at the ends of the column and less tilt amplitude of the column.

(6) Under PGA = 0.1 g, the curves of the vertical displacements of the ceiling exhibit a "W" shape and those of the bottom slab show a "M" shape. The increase of the vertical stiffness ratio results in higher relative deformation of the ceiling. However, the relative stiffness has little influence on the relative deformation of the bottom slab. Besides, the maximum horizontal relative displacements between slabs and maximum inter-story drift angles increase with the increase of the horizontal stiffness ratio.

Acknowledgments

The work presented in this paper was funded by the National Natural Science Foundation of China (Grant No. 52378381).

References

Bao, X.H., Xia, Z.F., Ye, G.L., Fu, Y.B. and Su, D. (2017), "Numerical analysis on the seismic behavior of a large metro subway tunnel in liquefiable ground", *Tunn. Undergr. Sp. Technol.*, 66, 91-106. https://doi.org/10.1016/j.tust.2017.04.005.

Bobet, A., Fernandez, G., Huo, H.B. and Ramirez, J. (2008), "A practical iterative procedure to estimate seismic-induced deformations of shallow rectangular structures", *Can. Geotech. J.*, **45**(7), 923-938. https://doi.org/10.1139/T08-026.

Chen, G.X., Chen, S., Zuo, X., Du, X.L., Qi, C.Z. and Wang, Z.H. (2015), "Shaking-table tests and numerical simulations on a subway structure in soft soil", *Soil Dyn. Earthq. Eng.*, 76, 13-28. https://doi.org/10.1016/j.soildyn.2014.12.012.

Chen, J.N., Xu, C.S., El Naggar, H.M. and Du, X.L. (2023), "Quantification of seismic performance index limits and evaluation of seismic fragility for a new rectangular prefabricated subway station structure", *Tunn. Undergr. Sp. Technol.*, 138. https://doi.org/10.1016/j.tust.2023.105183.

Chen, J.N., Xu, C.S., El Naggar, H.M. and Du, X.L. (2023), "Seismic response analysis of rectangular prefabricated subway station structure", *Tunn. Undergr. Sp. Technol.*, 131. https://doi.org/10.1016/j.tust.2022.104795.

Cheng, X.L. and Sun, Z.G. (2018), "Effects of Burial Depth on the Seismic Response of Subway Station Structure Embedded in Saturated Soft Soil", *Adv. Civil Eng.*, **2018**, 1-12. https://doi.org/10.1155/2018/8978467.

Chou, J.C. and Lin, E.G.E. (2020), "Incorporating ground motion effects into Sasaki and Tamura prediction equations of liquefaction-induced uplift of underground structures", *Geomech. Eng.*, **22**(1), 25-33. https://doi.org/10.12989/gae.2020.22.1.025.

Cui, Z.D., Huang, M.H., Hou, C.Y. and Yuan, L. (2023), "Seismic deformation behaviors of the soft clay after freezing-thawing", *Geomech. Eng.*, **34**(3), 303-316. https://doi.org/10.12989/gae.2023.34.3.303.

Cui, Z.D., Zhang, L.J. and Zhan, Z.X. (2023), "Dynamic shear modulus and damping ratio of saturated soft clay", *Geomech. Eng.*, **32**(4), 411-426. https://doi.org/10.12989/gae.2023.32.4.411.

Cui, Z.D., Zhang, L.J. and Zhan, Z.X. (2023), "Seismic response analysis of shallowly buried subway station in inhomogeneous clay site", *Soil Dyn. Earthq. Eng.*, **171**, 107986. https://doi.org/10.1016/j.soildyn.2023.107986.

Ebadi-Jamkhaneh, M., Homaioon-Ebrahimi, A., Kontoni, D.P.N. and Shokri-Amiri, M. (2021), "Numerical FEM assessment of soil-pile system in liquefiable soil under earthquake loading including soil-pile interaction", *Geomech. Eng.*, **27**(5), 465-479. https://doi.org/10.12989/gae.2021.27.5.465.

Gao, Z.D., Zhao, M., Huang, J.Q., Wang, W.W. and Du, X.L. (2022), "Effect of soil-rock interface position on seismic response of subway station structure", *Tunn. Undergr. Sp. Technol.*, **119**, 104255. https://doi.org/10.1016/j.tust.2021.104255.

Gomes, R.C. (2013), "Effect of stress disturbance induced by construction on the seismic response of shallow bored tunnels", *Comput. Geotech.*, **49**, 338-351. https://doi.org/10.1016/j.compgeo.2012.09.007.

Huo, H., Bobet, A., Fernández, G. and Ramírez, J. (2005), "Load transfer mechanisms between underground structure and surrounding ground: Evaluation of the failure of the Daikai Station", *J. Geotech. Geoenviron. Eng.*, **131**(12), 1522-1533. https://doi.org/10.1061/(ASCE)1090-0241(2005)131:12(1522).

Huo, H., Bobet, A., Fernández, G. and Ramírez, J. (2006), "Analytical solution for deep rectangular structures subjected to far-field shear stresses", *Tunn. Undergr. Sp. Technol.*, **21**(6), 613-625. https://doi.org/10.1016/j.tust.2005.12.135.

Huynh, V.Q., Nguyen, T.K. and Nguyen, X.H. (2021), "Seismic analysis of soil-structure interaction: Experimentation and modeling", *Geomech. Eng.*, **27**(2), 115-121. https://doi.org/10.12989/gae.2021.27.2.115.

Iida, H., Hiroto, T., Yoshida, N. and Iwafuji, M. (1996), "Damage to Daikai Subway Station", *Soils Found.*, **36**, 283-300. https://doi.org/10.3208/sandf.36.Special_283.

Jaber, L., Mezeh, R., Zein, Z., Azab, M. and Sadek, M. (2023), "Nonlinear numerical analysis of influence of pile inclination on the seismic response of soil-pile-structure system", *Geomech. Eng.*, **34**(4), 437-447. https://doi.org/10.12989/gae.2023.34.4.437.

Jiang, J.W., Hesham El Naggar, M., Xu, C.S. and Du, X.L. (2023), "Effect of parameters associated with soil-to-structure relative stiffness on seismic fragility curves of subway station", *Tunn. Undergr. Sp. Technol.*, **135**, 105057. https://doi.org/10.1016/j.tust.2023.105057.

Jiménez, G.A.L., Dias, D. and Jenck, O. (2022), "Seismic loading response of piled systems on soft soils - Influence of the Rayleigh damping", *Geomech. Eng.*, **29**(2), 155-170. https://doi.org/10.12989/gae.2021.27.2.115.

Li, Y.T., Di, H.G., Zhou, S.H. and Gong, Q.M. (2021), "Seismic Analysis for Cross Transfer Subway Stations in Soft Soil Stratum", *KSCE J. Civil Eng.*, **25**(5), 1732-1745. https://doi.org/10.1007/s12205-021-0634-4.

Lu, C.C. and Hwang, J.H. (2019), "Nonlinear collapse simulation of Daikai Subway in the 1995 Kobe earthquake: Necessity of dynamic analysis for a shallow tunnel", *Tunn. Undergr. Sp. Technol.*, **87**, 78-90. https://doi.org/10.1016/j.tust.2019.02.007.

Ma, C., Lu, D.C., Du, X.L., Qi, C.Z. and Zhang, X.Y. (2019), "Structural components functionalities and failure mechanism of rectangular underground structures during earthquakes", *Soil*

Dyn. Earthq. Eng., **119**, 265-280. https://doi.org/10.1016/j.soildyn.2019.01.017.

Miao, Y., Zhong, Y., Ruan, B., Cheng, K. and Wang, G.B. (2020), "Seismic response of a subway station in soft soil considering the structure-soil-structure interaction", *Tunn. Undergr. Sp. Technol.*, **106**, 103629. https://doi.org/10.1016/j.tust.2020.103629.

Seed, H.B. and Idriss, I.M. (1970), "Soil moduli and damping factors for dynamic response analyses", Report No.UCB/EERC-70/10, Earthquake Engineering Research Center, University of California at Berkeley, Berkeley, California.

Sun, Q.Q., Dias, D. and e Sousa, L.R. (2020), "Soft soil layer-tunnel interaction under seismic loading", *Tunn. Undergr. Sp. Technol.*, **98**, 103329. https://doi.org/10.1016/j.tust.2020.103329.

Tang, B.Z., Li, X.J., Chen, S., Zhuang, H.Y. and Chen, H.P. (2020), "Investigations of seismic response to an irregular-section subway station structure located in a soft clay site", *Eng. Struct.*, **217**, 110799. https://doi.org/10.1016/j.engstruct.2020.110799.

Tsinidis, G. (2017), "Response characteristics of rectangular tunnels in soft soil subjected to transversal ground shaking", *Tunn. Undergr. Sp. Technol.*, **62**, 1-22. https://doi.org/10.1016/j.tust.2016.11.003.

Wang, J.N. and Munfakh, G.A. (2001), "Seismic design of tunnels", *WIT Press*, 57. https://doi.org/10.2495/ERES010551.

Wang, W.L., Wang, T.T., Su, J.J., Lin, C.H., Seng, C.R. and Huang, T.H. (2001), "Assessment of damage in mountain tunnels due to the Taiwan Chi-Chi Earthquake", *Tunn. Undergr. Sp. Technol.*, **16**, 133-150. https://doi.org/10.1016/S0886-7798(01)00047-5.

Wu, W.F., Ge, S.F. and Yuan, Y. (2022), "Seismic response characteristics of cross interchange metro stations: Transversal response of the three-storey section", *Eng. Struct.*, **252**, 113525. https://doi.org/10.1016/j.engstruct.2021.113525.

Wu, W.F., Ge, S.P., Yuan, Y., Ding, W.Q. and Anastasopoulos, I. (2021), "Seismic response of a cross interchange metro station in soft soil: Physical and numerical modeling", *Earthq. Eng. Struct. D.*, **50**(9), 2294-2313. https://doi.org/10.1002/eqe.3446.

Xu, Z.G., Du, X.L., Xu, C.S., Hao, H., Bi, K.M. and Jiang, J.W. (2019), "Numerical research on seismic response characteristics of shallow buried rectangular underground structure", *Soil Dyn. Earthq. Eng.*, **116**, 242-252. https://doi.org/10.1016/j.soildyn.2018.10.030.

Yu, H.T., Chen, J.T., Bobet, A. and Yuan, Y. (2016), "Damage observation and assessment of the Longxi tunnel during the Wenchuan earthquake", *Tunn. Undergr. Sp. Technol.*, **54**, 102-116. https://doi.org/10.1016/j.tust.2016.02.008.

Zhang, C.L. and Cui, Z.D. (2017), "Numerical simulation of dynamic response around shield tunnel in the soft soil area", *Mar. Georesour. Geotec.*, **35**(7), 1018-1027. https://doi.org/10.1080/1064119x.2016.1278063.

Zhuang, H.Y., Hu, Z.H., Wang, X.J. and Chen, G.X. (2015), "Seismic responses of a large underground structure in liquefied soils by FEM numerical modelling", *Bull. Earthq. Eng.*, **13**(12), 3645-3668. https://doi.org/10.1007/s10518-015-9790-6.

Zhuang, H.Y., Ren, J.W., Miao, Y., Jing, L.G., Yao, E.L. and Xu, C.J. (2019), "Seismic performance levels of a large underground subway station in different soil foundations", *J. Earthq. Eng.*, **25**(14), 2808-2833. https://doi.org/10.1080/13632469.2019.1651423.